Iranian Journal of Numerical Analysis and Optimization
Vol. 16, No. 3, 2026, pp 1107–1132
https://doi.org/10.22067/ijnao.2026.97170.1815
https://ijnao.um.ac.ir/

Research Article

Analysis of 2D Burger's equation using numerical and semi-analytic techniques

A. Kaur, A. Pasrija and S. Arora*

Abstract

The effect of advective and diffusive components is studied using the 2D Burgers' equation. The diffusive term is influenced by the Reynolds number. Spatial discretization is performed using radial basis collocation, while the temporal direction is discretized using 4th Runge–Kutta method. To analyze the error behavior, the closed-form solution of 2D Burgers' equation is derived analytically using a generalized bivariate homotopy perturbation approach. A comprehensive discussion and comparison of both numerical and semi-analytical solutions are presented in terms of absolute error, as well as $\|e\|_\infty$ and $\|e\|_2$ error norms. The effect of Reynolds number on the diffusion component is illustrated graphically. Algorithms for both numerical and analytical techniques have been implemented in MATLAB R2023.

AMS subject classifications (2020): Primary 65D12, 65N12; Secondary 35B25, 65N35.

*Corresponding author

Received 24 December 2025; revised 21 April 2026; accepted 29 April 2026

Amandeep Kaur
Department of Mathematics, Punjabi University, Patiala-147002, Punjab, India. e-mail: amandeepk_rs23@pbi.ac.in

Atul Pasrija
Department of Computer Applications, CGC, Landran, Mohali-140307, Punjab, India. e-mail: atulpasrija94678@gmail.com

Shelly Arora
Department of Mathematics, Punjabi University, Patiala-147002, Punjab, India. e-mail: aroshelly@gmail.com

How to cite this article
Kaur, A., Pasrija, A. and Arora, S., Analysis of 2D Burger's equation using numerical and semi-analytic techniques. *Iran. J. Numer. Anal. Optim.*, 2026; 16(3): 1107-1132. https://doi.org/10.22067/ijnao.2026.97170.1815

Keywords: Radial basis functions, Runge–Kutta method, GB transform, Burger's equation.

1 Introduction

The transport phenomenon in advection-diffusion equation is best represented by Navier–Stokes equation. It represents the transfer of heat and energy from one medium to another. Burger's equation is a special case of Navier Stoke's equation. This equation has numerous applications in fluid dynamics, physics, solid state physics, aeronautics, turbulence theory, and so on. Bateman [6] developed Burger's equation from Navier–Stokes by excluding the pressure gradient term and later, in 1948, Burger has redefined it. In the present scenario, the application of Burger's equation is not confined to fluid dynamics, also includes traffic flow [11], cosmology [44], gas dynamics [9], acoustics [29], continuous stochastic processes [10], electromagnetic waves [27] and many more.

The advective and diffusive components are represented by nondissipative hyperbolic component and the dissipative parabolic component, respectively.

Consider the two-dimensional (2D) Burgers' equation defined on a bounded domain Ω as follows:

$$\vartheta_t + \alpha\vartheta\nabla\vartheta - \frac{1}{Re}\nabla^2\vartheta = f(X,t),\ X \in \Omega \subset \mathbb{R}^2, \quad t \geq 0, \tag{1}$$

where ∇ is the gradient operator and ∇^2 is the Laplacian operator, Re represents the Reynolds number, α is any parameter such that $\alpha \geq 0$, and $f(X,t)$ are a continuous function defined on the domain Ω and for $t \geq 0$. The initial condition is defined as follows:

$$\vartheta(X,0) = \psi(X), \qquad X \in \Omega, \tag{2}$$

and the boundary conditions are defined as

$$\mathcal{B}\vartheta(X,t) = \phi(X,t), \qquad X \in \partial\Omega,\ t \geq 0, \tag{3}$$

where the function ϑ describes advection and diffusion quantities such as heat, mass, energy , and so on, over the spatial domain Ω at time $t \geq 0$, and $\mathcal{B}$ represents the boundary operator on the boundary of the spatial domain. The nonlinear term with ∇ operator accounts for advection and Re is the Reynolds number, which is inversely proportional to the viscosity parameter that measures the rate of diffusion. Moreover, $\psi(X)$ is the bounded function defined on the domain Ω and $\phi(X,t)$ are continuous functions defined on the boundary $\partial\Omega$.

The linear advection-diffusion equation has been studied in [35] through the framework of finite elements. The coupling of nonstandard finite difference and Haar wavelets with quasi-linearization for a class of generalized Burger's equations has been discussed in [26]. Polynomial differential quadrature method with Runge–Kutta (RK)4 was implemented in [31] to obtain the numerical results for one-dimensional D and 2D Burgers' equation systems. Nonuniform grid friendly localized differential quadrature method was proposed in [4] to solve viscous Burger's equation in one and two dimensions. Fully implicit finite difference scheme was discussed in [5, 21] for 2D Burger's equation.

Nevertheless, scholars have contributed with several analytic methods to determine the explicit solutions of linear and nonlinear advection-diffusion equation such as [33, 32, 1]. There are several other numerical techniques followed by investigators to solve Burger's equation such as the sine and cosine method [22], inverse scattering technique [17], the simplest equation technique [36], extended simplest equation technique [8], Kudryashov method [23], Backlund transformation technique [19], exp-function technique [30], Hirota's method [43], homogeneous balance technique [20], bifurcation method [28], Darboux transformation [45], G'/ G-expansion technique [34], Lie group analysis [42] and weighted finite difference method [37] and so on.

In the present study, the semi-analytic and numerical perspectives have been explored by generalized bivariate homotopy perturbation method (GB-HPM) and 4th order RK method, respectively, with mesh-less approach based on radial basis functions (RBFs).

2 Radial basis functions

Conventional mesh generates methods such as finite difference, finite element and spectral methods suffer from the complexity of mesh-generation for multidimensional problems. Alleviating the labor of mesh-generation, mesh-less methods are developed with enough flexibility to extend their applicability to irregular geometries, scattered and multivariate data. RBFs with collocation method have become an important tool to study the multidimensional problems.

RBFs were first introduced by Hardy [18] to study the topographical mapping. Later on the origination of Kansa's work on collocation technique with RBFs revolutionized the perspective of the study of partial differential equations using RBFs [24]. These functions basically, represent the distance between the node point $\mathbf{X_i}$ and the data point $\mathbf{X}$ and are independent of the space dimension and isotropy. In simple words RBFs are univariate function whose value depend upon distance between the point and the center point of the function. An RBF can be defined as follows:

A function $\Phi : \mathcal{R}^d \to \mathcal{R}$ is said to be RBF if there exists a radial distance r such that $r = \|X - X_k\|$ which implies $r = \sqrt{(\xi - \xi_k)^2 + (\zeta - \zeta_k)^2}$ and $\Phi(X) = \Phi(r)$, where $\|.\|$ denotes Euclidean norm.
By the time, various RBFs have been developed to study the partial differential equations such as Gaussian (GA), multiquadric (MQ), inverse multiquadric (IMQ), and so on. The list of commonly used RBFs is given in Table 1. From this table, it is observed that an unknown parameter ν is introduced which is a free parameter, commonly known as the shape parameter.

Table 1: List of RBFs

RBFs	Definition
GA	$\Phi(\mathbf{r}) = e^{-(\nu\mathbf{r})^2}$
MQ	$\Phi(\mathbf{r}) = \sqrt{1+(\nu\mathbf{r})^2}$
IMQ	$\Phi(\mathbf{r}) = \frac{1}{\sqrt{1+(\nu\mathbf{r})^2}}$
Inverse quadric	$\Phi(\mathbf{r}) = \frac{1}{1+(\nu\mathbf{r})^2}$
Thin plate spline	$\Phi(\mathbf{r}) = \mathbf{r}^2 ln(\mathbf{r})$
Monomial	$\Phi(\mathbf{r}) = \mathbf{r}^{2k-1}; k \in N$

Shape parameter

Along with the choice of RBFs, the shape parameter possesses great influence on the accuracy and condition number of the coefficient matrix of RBFs [40]. Infinitely smooth RBFs such as MQ and GA manifest exponential convergence as the shape parameter approaches infinity. However, it further leads to high condition number associated with ill-conditioning of the system. The open problem of selecting optimal shape parameter has engrossed several studies with generation of different criterion to investigate the good choice of shape parameter. Trial and error method is most common in practice to pick the best shape parameter that has least error. When exact solution is not given for 2D problems following strategies have been adopted to choose the shape parameter.
Hardy [18] suggested the shape parameter for IMQ RBFs as

$$\nu = \frac{1}{0.815d}, \qquad d = \frac{1}{N}\sum_{j=1}^{N} d_j,$$

where N is the number of data points and d_j represents the distance to the nearest data point in neighbor.

Franke [16] formulated shape parameter for 2D systems as

$$\nu = \frac{0.8\sqrt{N}}{D},$$

where D is the diameter of the smallest circle which includes all data points.

Fasshauer [14] elaborated the good choice for shape parameter as

$$\nu = \frac{2}{\sqrt{N}}.$$

In [14], these strategies are remarked as optional for very specific examples and certainly cannot be considered as general instructions. Carlson and Foley [13] stated the shape parameter as problem dependent. Borrowing idea from method of cross validation practiced in statistics literature, Rippa [39] proposed special case of leave-one-out cross validation to circumvent the issue of selecting optimal shape parameter in context of interpolating scattered data with RBFs. Moreover, Fasshauer and Zhang [15] reviewed LOOCV and introduced its extension for pseudo-spectral methods for solving partial differential equations. Biazar and Hosami [7] discussed the strategy to find an interval for the optimal shape parameter rather than constant value. The leading stumbling block of global collocation is the severe ill-conditioning of the system matrix. Using a greater value for shape parameter leads to the ill-conditioned interpolation matrix, with a condition number grows exponentially large. Addressing this issue, in [25], authors have remarked on the tolerance of RBFs for a large condition number of matrix upto $\mathcal{O}(10^{16})$ within machine double precision. The ill-conditioning has a significant impact on the results.This behavior is called the uncertainty principle. The present study relies on the algorithm drawn in Algorithm 1.

Algorithm 1 Algorithm for Shape Parameter

```
Input: CD_min, CD_max, ν_increment
CD = 1
while CD > CD_max and CD < CD_min do
    form required matrix say  ;
    use P,Q,R = svd( );
    CD = Q(1,1)/Q(end,end);
    if CD < CD_min then ν = ν - ν_increment;
    else if  CD > CD_max then ν = ν + ν_increment;
    end if
end while
Output: ν
```

3 Implementation of RBFs with collocation method

Collocation technique is one of the weighted residual method in which the residual is set equal to zero at collocation points. Therefore, in RBF collocation method, the node points are taken to be the collocation points. The unconditional positive definite feature of GA RBFs guarantees the solvability of the resulting system which ensures the implementation of GA as base functions to implement the collocation technique. In the present study, the GA RBF Φ_k has been proposed to define the trial function. The GA RBFs are defined as:

$$\Phi_k(r) = \exp(-\nu^2 r^2), \qquad k = 1, 2, \ldots, N, \tag{4}$$

where $r = \sqrt{(\xi - \xi_k)^2 + (\zeta - \zeta_k)^2}$, $k = 1, 2, \ldots, N$.

Let $\bar{\vartheta}$ be the approximation of $\vartheta(r, t)$ in terms of GA RBFs Φ with a given set of node points $\{X_1, X_2, \ldots, X_N\} \subset \Omega$ can be expressed as

$$\bar{\vartheta} = \sum_{k=1}^{N} \Phi_k(r) C_k(t), \tag{5}$$

where C_k's are unknown coefficients and N is the number of collocation points which coincide with the node points. The node points r are given by $r = \|X - X_k\| = \sqrt{(\xi - \xi_k) + (\zeta - \zeta_k)^2}$.

The adjustment of node points is the main task to implement the collocation technique. Let N_{int} be the node points in the interior of the domain and let N_b be the node points on the boundary such that the total number of node points is $N = N_{int} + N_b$. The uniform distribution of node points is shown in Figure 1 for $N = 400$ and the flowchart for shape parameter is given in Figure 2. The trial function $\vartheta(r, t)$ at time t_p and the jth node point can be written as

$$\bar{\vartheta}_j^p = \sum_{k=1}^{N} \Phi_k(r_j) C_k^p, \qquad j = 1, 2, \ldots, N. \tag{6}$$

In the matrix form, (6) can be written as

$$\vartheta(r_j, t_p) = \ ., \tag{7}$$

where ${}_{\mathbf{j,k}} = \left[\Phi_k(r_j)\right]_{N \times N}$, $1 \le j, k \le N$ is the matrix of RBFs and $\ = [C_1^p, C_2^p, \ldots, C_N^p]'$ denotes the vector of expansion coefficients. The RBF matrix is defined below:

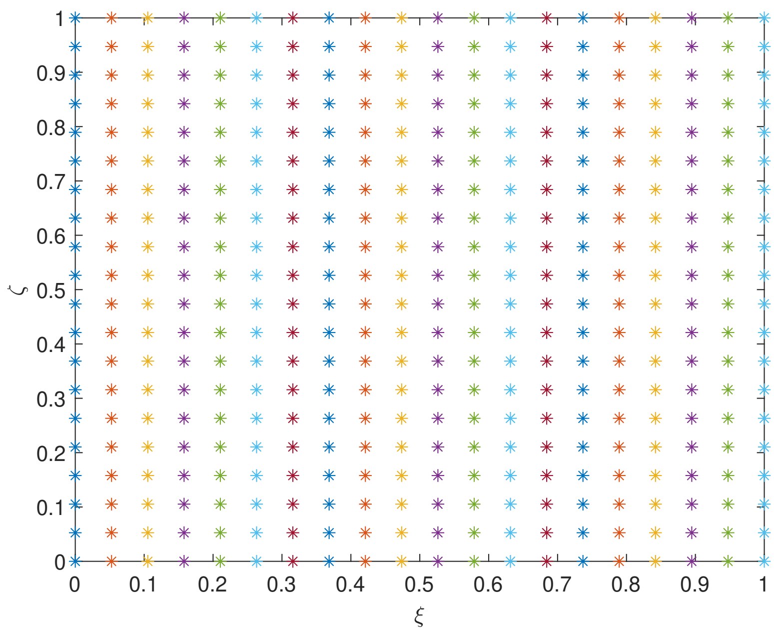

Figure 1: Uniform point distribution for N = 400.

$$\begin{bmatrix} \Phi_1(r_1) & \Phi_2(r_1) & \Phi_3(r_1) & \dots & \Phi_N(r_1) \\ \Phi_1(r_2) & \Phi_2(r_2) & \Phi_3(r_2) & \dots & \Phi_N(r_2) \\ \Phi_1(r_3) & \Phi_2(r_3) & \Phi_3(r_3) & \dots & \Phi_N(r_3) \\ \vdots & \vdots & \vdots & \ddots & \vdots \\ \Phi_1(r_N) & \Phi_2(r_N) & \Phi_3(r_N) & \dots & \Phi_N(r_N) \end{bmatrix},$$

where $\Phi_k(r_j) = \exp(-\nu^2 r_j^2)$ and $r_j = \sqrt{(\xi_j - \xi_k)^2 + (\zeta_j - \zeta_k)^2}$.

4 Temporal discretization using 4th order Runge–Kutta Method

Implementing (6) on (1) and (3) at t_p, the following system of equations is obtained:

$$\sum_{k=1}^{N} \Phi_{jk} \frac{dC_k}{dt} = \frac{1}{Re} \sum_{k=1}^{N} \nabla^2(\Phi_{jk}) C_k - \alpha \sum_{k=1}^{N} \Phi_{jk} C_k(t) \sum_{k=1}^{N} \nabla(\Phi_{jk}) C_k + f(X_j, t), \tag{8}$$
$$j = 1, 2, \dots, N_{int}.$$

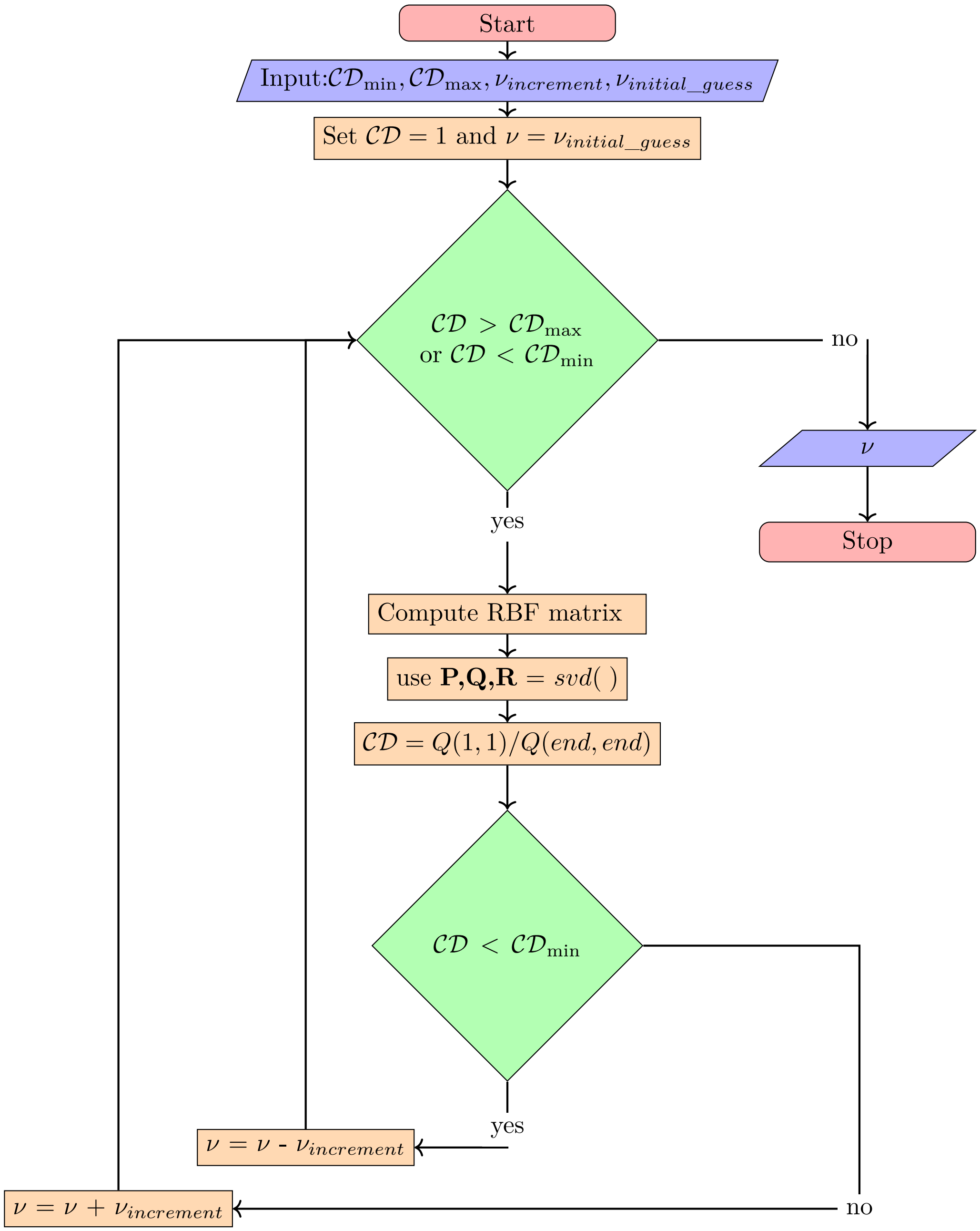

Figure 2: Flowchart of pseudo code for optimal shape parameter

The boundary conditions can be imposed as

$$\mathcal{B}\sum_{k=1}^{N}\Phi_{mk}C_k = \phi(r_m,t), \qquad m = 1,2,\dots,N_b. \tag{9}$$

In matrix form, (8) and (9) can be written as

$$\frac{\partial}{\partial t} = \frac{1}{Re}\big(\nabla^2 \ \big) \ -\alpha\big(\ \ \big)\big(\nabla(\ )\ \big) + f(X_j,t). \tag{10}$$

By replacing appropriate rows corresponding to the indexing of boundary points in (10), imposed boundary conditions and setting the equations in differential form the 4th order RK method is applied.

To control the step-size (δt), the algorithm of RK method of order 4 is presented with flowchart. Hence, present study follows 4th order Runge–Kutta method given as

$$\begin{aligned}
\mathcal{S}_1 =& \delta t\mathcal{F}(t_p,\vartheta_j^p),\\
\mathcal{S}_2 =& \delta t\mathcal{F}(t_p+\frac{\delta t}{2},\vartheta_j^p+\frac{\mathcal{S}_1}{2}),\\
\mathcal{S}_3 =& \delta t\mathcal{F}(t_p+\frac{\delta t}{2},\vartheta_j^p+\frac{\mathcal{S}_2}{2}),\\
\mathcal{S}_4 =& \delta t\mathcal{F}(t_p+\delta t,\vartheta_j^p+\mathcal{S}_3),\\
\vartheta_j^{p+1} =& \vartheta_j^p+\frac{\delta t}{6}(\mathcal{S}_1+2\mathcal{S}_2+2\mathcal{S}_3+\mathcal{S}_4).
\end{aligned} \tag{11}$$

The algorithm and flowchart of RBF with 4th order RK method is given in Algorithm 2 and Figure 3, respectively.

Algorithm 2 Algorithm for 4th order Runge–Kutta method

Input: $t_0, t_f, \delta t$
% t_0 = initial time, t_f = finial time, δt = step size,
$T = t_0 : \delta t : t_f$
for j = 1:length of T **do**

$$\begin{aligned}
\mathcal{S}_1 =& \delta t\mathcal{F}(t_p,\vartheta_j^p),\\
\mathcal{S}_2 =& \delta t\mathcal{F}(t_p+\frac{\delta t}{2},\vartheta_j^p+\frac{\mathcal{S}_1}{2}),\\
\mathcal{S}_3 =& \delta t\mathcal{F}(t_p+\frac{\delta t}{2},\vartheta_j^p+\frac{\mathcal{S}_2}{2}),\\
\mathcal{S}_4 =& \delta t\mathcal{F}(t_p+\delta t,\vartheta_j^p+\mathcal{S}_3),\\
\vartheta_j^{p+1} =& \vartheta_j^p+\frac{\delta t}{6}(\mathcal{S}_1+2\mathcal{S}_2+2\mathcal{S}_3+\mathcal{S}_4)
\end{aligned}$$

end for
Output:ϑ_j^{p+1}

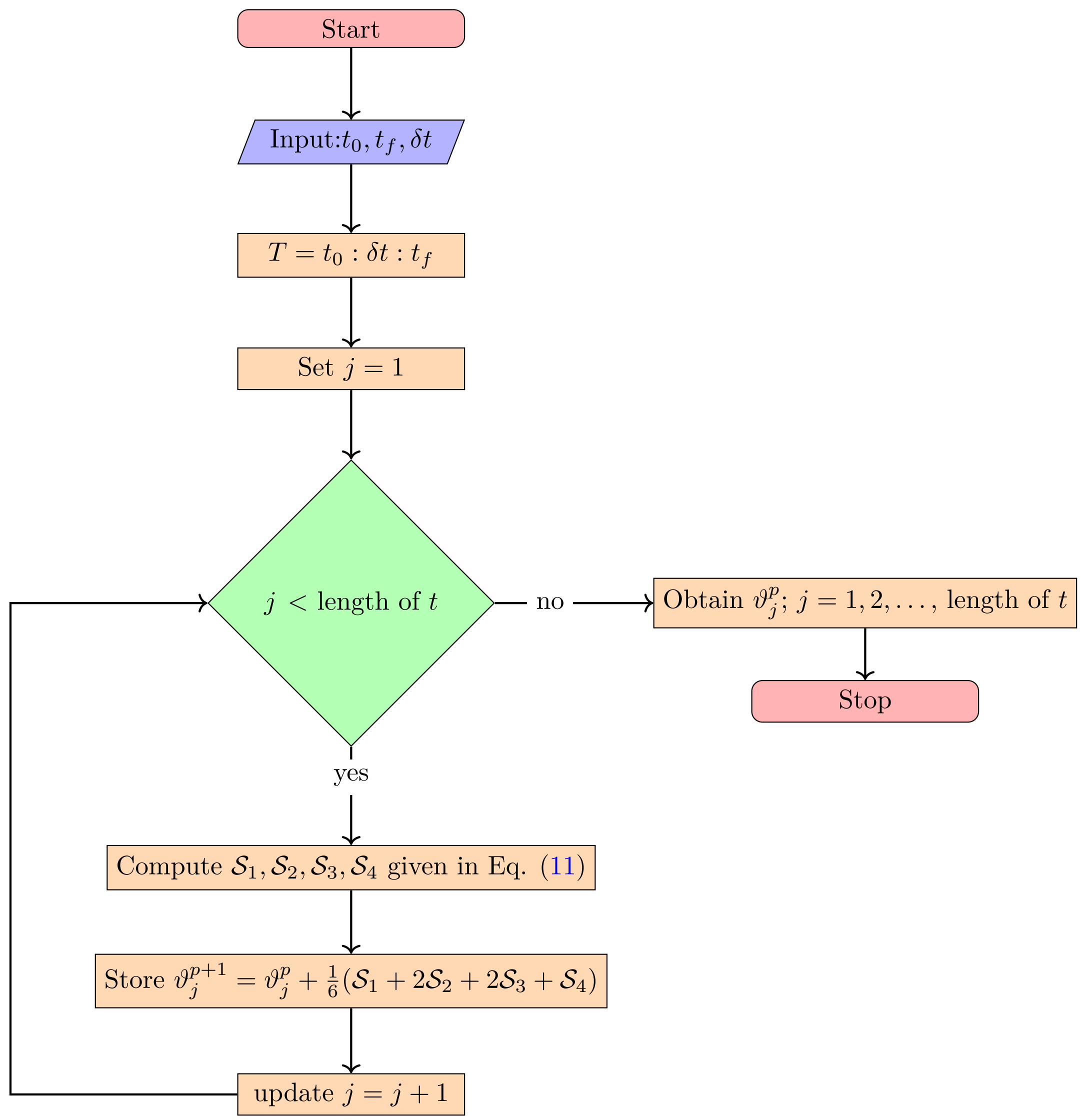

Figure 3: Flowchart of pseudo code for 4th order RK method

5 Generalized bivariate homotopy perturbation method

The analytical approach produces an exact solution that reflects the qualitative behavior of the model problem. Inefficiency of existing analytic approaches for complex problems shifts the preference to numerical approaches which deliver approximate quantitative data for selected points. The middle course of both approaches, as mentioned before, is a semi-analytic approach. It is based on the methodology of the expansion method and assumes results in the form of a series and evaluates the subsequent component of the series with the prior one. The hybrid approach of GB-HPM, inherits the merits of both analytic and approximation methodologies. It yields the exact solution through the closed form of the approximate series solution. Some of the primary results of the GB transform are as follows:

Definition 1. [2] The GB transform of function $\vartheta\left(X,t\right)$ with respect to t is given by

$$\mathcal{G}_m\left(\vartheta\left(X,t\right)\right)=\mathcal{B}_m\left(X,s,\gamma\right)=\frac{s}{\gamma^m}\int_0^\infty t^{m-1}\exp\left(-\frac{s}{\gamma}t\right)\vartheta\left(X,t\right)dt, \tag{12}$$

where m is the order and s and γ are transformation variable.

Definition 2. [2] If $\mathcal{B}_m\left(s,\gamma\right)$ is the GB transform of function $\vartheta\left(X,t\right)$, then the inverse GB transform of $\mathcal{B}_m\left(X,s,\gamma\right)$ is $\vartheta\left(X,t\right)$ such that

$$\mathcal{G}_m^{-1}\left(\mathcal{B}_m\left(X,s,\gamma\right)\right)=\vartheta\left(X,t\right). \tag{13}$$

Theorem 1. [2] Let $\vartheta(X,t),\vartheta'(X,t),\dots,\vartheta^{m-1}(X,t)$ be continuous and of exponential order on $[0,\infty)$ while $\vartheta^n(X,t)$ is piece-wise continuous on $[0,\infty)$ with respect to t. Then

$$\begin{aligned}\mathcal{G}_m[\vartheta^n(X,t)]=&(-1)^{m-1}\\&\times\frac{s}{\gamma}\frac{\partial^{m-1}}{\partial s^{m-1}}\left[\left(\frac{s}{\gamma}\right)^{n-1}\mathcal{G}_1[\vartheta(X,t)]-\sum_{k=0}^{n-1}\left(\frac{s}{\gamma}\right)^{n-(k+1)}\vartheta^k(X,0)\right].\end{aligned}$$

The pseudo code of the GB-HPM is defined in Algorithm given in Figure 4. Applying GB transform of order one on (1) yields

$$\mathcal{G}_1[\vartheta(X,t)]=\vartheta(X,0)\frac{\gamma}{s}\mathcal{G}_1\left[\alpha\vartheta\nabla\vartheta-\frac{1}{Re}\nabla^2\vartheta\right]. \tag{14}$$

Operating inverse of GB transform on (14) gives

$$\vartheta(X,t)=\vartheta(X,0)-\mathcal{G}_1^{-1}\left\{\frac{\gamma}{s}\mathcal{G}_1\left[\alpha\vartheta\nabla\vartheta-\frac{1}{Re}\nabla^2\vartheta\right]\right\}. \tag{15}$$

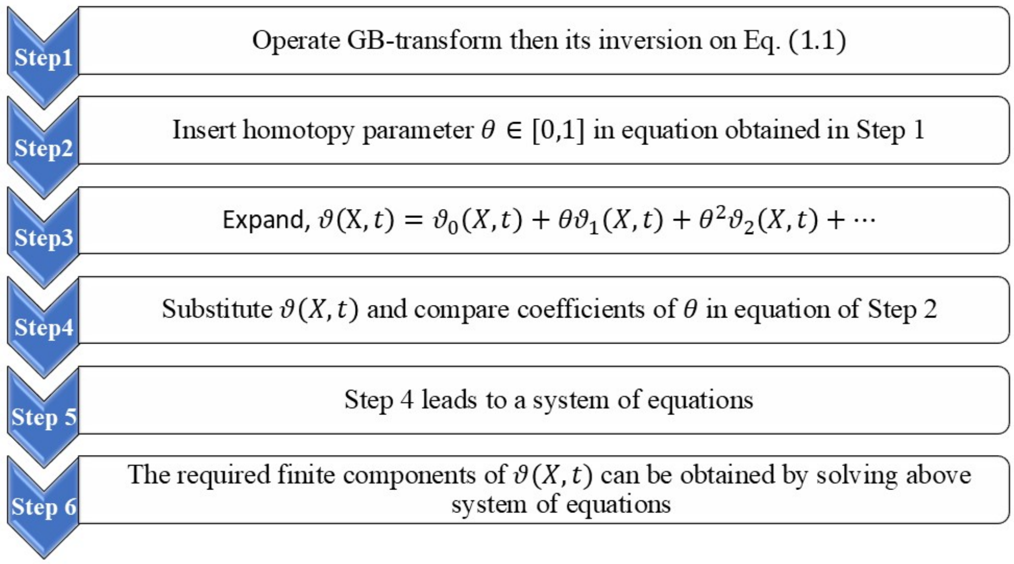

Figure 4: Algorithm for GB-HPM.

To form homotopic equation, insert homotopy parameter $\theta \in [0,1]$ (15) as follows:

$$\vartheta(X,t) = \vartheta(X,0) - \theta\mathcal{G}_1^{-1}\left\{\frac{\gamma}{s}\mathcal{G}_1\left[\alpha\vartheta\nabla\vartheta - \frac{1}{Re}\nabla^2\vartheta\right]\right\}. \tag{16}$$

Assume that the solution of (16) can be expanded as

$$\vartheta(X,t) = \vartheta_0(X,t) + \theta\vartheta_1(X,t) + \theta^2\vartheta_2(X,t) + \cdots\ . \tag{17}$$

Substituting (17) in (16) and comparing the coefficients of θ^n (for $n = 0,1,2,\ldots$) result the following system of equations:

$$\begin{aligned}
&\vartheta_0(X,t) = \vartheta(X,0),\\
&\vartheta_1(X,t) = \mathcal{G}_1^{-1}\left\{\frac{\gamma}{s}\mathcal{G}_1\left[\alpha\vartheta_0\nabla\vartheta_0 - \frac{1}{Re}\nabla^2\vartheta_0\right]\right\},\\
&\vartheta_2(X,t) = \mathcal{G}_1^{-1}\left\{\frac{\gamma}{s}\mathcal{G}_1\left[\alpha(\vartheta_0\nabla\vartheta_1 + \vartheta_1\nabla\vartheta_0) - \frac{1}{Re}\nabla^2\vartheta_1\right]\right\},
\end{aligned} \tag{18}$$

$$\vdots$$

$$\vartheta_n(X,t) = \mathcal{G}_1^{-1}\left\{\frac{\gamma}{s}\mathcal{G}_1\left[\sum_{k=0}^{n}\alpha\vartheta_k\nabla\vartheta_{n-k-1} - \frac{1}{Re}\nabla^2\vartheta_{n-1}\right]\right\}.$$

Computing the component of above system of equations yields the required series solution (17). For more details of GB-HPM, readers are advised to read [2, 3]. The semi-analytic solutions of different problems under different conditions are presented in the succeeding section.

6 Implementation of numerical and analytic techniques

The implementation of any technique whether it is analytic or numerical is a vital part of the study to ensure its application and the verification under different conditions. In this section, the numerical tests for proposed semi-analytic and numerical procedures are presented. The comparison of numerical and analytic techniques is presented in terms of error analysis defined below:

$$\begin{aligned} Abs &= |\vartheta_j^p - \tilde{\vartheta}_j^p|, \\ \|e\|_\infty &= \max_j |\vartheta_j^p - \tilde{\vartheta}_j^p|, \\ \|e\|_2 &= \sqrt{\frac{1}{N}\sum_{j=1}^{N}\left(\vartheta_j^p - \tilde{\vartheta}_j^p\right)^2}, \end{aligned}$$

where ϑ_j^p and $\tilde{\vartheta}_j^p$ are exact and approximate solutions, respectively, computed at $X_j \in \Omega$ and $t_p \in [0,T]$.

Example 1. Consider the unsteady viscous 2D Burger's equation:

$$\frac{1}{Re}(\vartheta_{\xi\xi} + \vartheta_{\zeta\zeta}) = \vartheta_t + \alpha\vartheta(\vartheta_\xi + \vartheta_\zeta), \qquad 0 < \xi, \zeta < 1, t > 0. \tag{19}$$

For the specific case $\alpha = 1$, the analytic solution is mentioned in [31, 38]as follows:

$$\vartheta(\xi,\zeta,t) = \frac{1}{\exp\left(\frac{Re(\xi+\zeta-t)}{2}\right)}, \tag{20}$$

The initial and boundary conditions are obtained from (20).

According to the description of the of GB-HPM given in Section 2.1, the component of semi-analytic series solutions are obtained as

$$\vartheta_0(\xi,\zeta,t) = 1/(\exp((Re(\xi+\zeta))/2)+1),$$
$$\vartheta_1(\xi,\zeta,t) = Ret\exp((Re(\xi+\zeta))/2)\Big(2\alpha+\frac{\exp((Re(\xi+\zeta)/2)-1))}{2(\exp((Re(\xi+\zeta))/2)+1)^3}\Big),$$
$$\begin{aligned}\vartheta_2(\xi,\zeta,t) = (&Re^2t^2\exp((Re(\xi+\zeta))/2)(4\alpha-11\exp(Re(\xi+\zeta))\\ &+11\exp((Re(\xi+\zeta))/2)+\exp((3Re(\xi+\zeta))/2)\\ &+12\alpha\exp(Re(\xi+\zeta))-24\alpha\exp((Re(\xi+\zeta))/2)\\ &+12\alpha^2\frac{\exp((Re(\xi+\zeta))/2)-4\alpha^2-1))}{(8(\exp((Re(\xi+\zeta))/2)+1)^5)},\\ &\vdots\end{aligned}$$

Furthermore, for $n \geq 2$, desired number of terms of series solution can be obtained to enhance its accuracy. The numerical values listed in Table 2 are calculated at various time levels t for different numbers of collocation points N and step size δt. Table 3 demonstrates better accuracy as value of N increases for high Reynolds numbers that have been not considered yet and it displays superior outcomes than available in literature for $Re = 100$. It is observed from these tables that even Reynolds number increases, the error norms remain stable and does not fluctuate or diverge, which shows the applicability of technique on the proposed problem.

Table 2: Error norms of RBF-RK solutions of Example 1 for $\alpha = 1$ and $Re = 10$ at various time levels.

			$t = 0.05$		$t = 0.25$		$t = 0.5$	
Method	N	δt	$\lVert e\rVert_\infty$	$\lVert e\rVert_2$	$\lVert e\rVert_\infty$	$\lVert e\rVert_2$	$\lVert e\rVert_\infty$	$\lVert e\rVert_2$
RBF-RK	100	0.005	2.2342e-05	6.4207e-06	1.5028e-04	3.0529e-05	1.3028e-04	3.9193e-05
	400	0.001	3.2139e-06	4.0586e-07	1.3798e-05	1.5346e-06	9.3718e-06	3.0963e-06
FIFD [33]	900	0.005	9.3799e-05	1.6417e-05	2.3733e-04	5.2981e-05	-	-
MTCB-DQM [1]	3600	0.0001	6.9200e-05	1.1600e-05	5.3000e-05	1.5100e-05	5.2600e-05	1.8800e-05

Table 3: Error norms of RBF-RK solutions of Example 1 at $\alpha = 1$ and $t = 0.05$ with $\delta t = 0.001$ for various Re.

		$Re = 100$		$Re = 200$	
Method	N	$\lVert e\rVert_\infty$	$\lVert e\rVert_2$	$\lVert e\rVert_\infty$	$\lVert e\rVert_2$
RBF-RK	25	1.2067e-07	2.8168e-08	7.5064e-08	1.7538e-08
	36	5.2821e-08	2.0907e-08	1.7069e-08	1.1214e-08
BBFE [32]	25	3.2143e-06	3.4403e-06	-	-
	441	2.0547e-06	2.3549e-06	-	-
		$Re = 500$		$Re = 700$	
		$\lVert e\rVert_\infty$	$\lVert e\rVert_2$	$\lVert e\rVert_\infty$	$\lVert e\rVert_2$
RBF-RK	25	3.3011e-08	7.7190e-09	2.3994e-08	5.6116e-09
	36	7.4839e-09	4.9135e-09	5.4365e-09	3.5689e-09

In Tables 4 and 5, numerical values are tabulated by considering initial five terms of GB-HPM series solution. Semi-analytic GB-HPM is distinguished at small time level $t = 0.01$. However, it faces challenges as time marched to $t = 0.5$. The numerical RBF-RK with $N = 400$ and $\delta t = 0.001$ performs quite well where absolute error ranges from 10^{-5} to 10^{-8}.

Table 4: Numerical results and absolute errors of solutions of Example 1 at $\alpha = 1$ and $Re = 10$.

t	ξ	ζ	GB-HPM	RBF-RK	Abs_{GB-HPM}	Abs_{RBF-RK}
0.01	0.1	0.1	2.78884e-01	2.7888e-01	1.26684e-10	4.0228e-07
	0.5	0.1	4.97365e-02	4.9733e-02	1.38650e-11	3.1659e-06
	0.9	0.1	7.03358e-03	7.0314e-03	1.40396e-11	2.2335e-06
	0.3	0.3	4.97365e-02	4.9734e-02	1.38650e-11	2.5540e-06
	0.7	0.3	7.03358e-03	7.0303e-03	1.40396e-11	3.3208e-06
	0.1	0.5	4.97365e-02	4.9735e-02	1.38650e-11	1.0479e-06
	0.5	0.5	7.03358e-03	7.0318e-03	1.40396e-11	1.7792e-06
	0.9	0.5	9.57717e-04	9.5640e-04	2.32464e-12	1.3206e-06
	0.1	0.9	7.03358e-03	7.0334e-03	1.40396e-11	2.0050e-07
	0.9	0.9	1.29720e-04	1.2978e-04	3.22787e-13	5.6619e-08
0.5	0.1	0.1	7.51387e-01	8.1757e-01	6.61867e-02	2.7296e-07
	0.5	0.1	4.04386e-01	3.7755e-01	2.68453e-02	5.0835e-06
	0.9	0.1	7.02560e-02	7.5855e-02	5.60212e-03	2.8064e-06
	0.3	0.3	4.04386e-01	3.7754e-01	2.68453e-02	2.5281e-06
	0.7	0.3	7.02560e-02	7.5860e-02	5.60212e-03	2.3182e-06
	0.1	0.5	4.04386e-01	3.7754e-01	2.68453e-02	9.5033e-08
	0.5	0.5	7.02560e-02	7.5862e-02	5.60212e-03	4.0642e-06
	0.9	0.5	9.84591e-03	1.0989e-02	1.14103e-03	2.3675e-06
	0.1	0.9	7.02560e-02	7.5857e-02	5.60212e-03	8.8786e-07
	0.9	0.9	1.33883e-03	1.5056e-03	1.62345e-04	4.3955e-06

Table 5: Numerical results of Example 1 at $t = 0.01$ and $Re = 10$ for different α.

		$\alpha = 0$		$\alpha = 2$	
ξ	ζ	GB-HPM	RBF-RK	GB-HPM	RBF-RK
0.1	0.1	2.7334E-01	2.7347e-01	2.8474e-01	2.8453e-01
0.5	0.1	4.9493E-02	4.9491e-02	4.9984e-02	4.9985e-02
0.9	0.1	7.0284E-03	7.0188e-03	7.0388e-03	7.0440e-03
0.3	0.3	4.9493E-02	4.9484e-02	4.9984e-02	4.9993e-02
0.7	0.3	7.0284E-03	7.0359e-03	7.0388e-03	7.0305e-03
0.1	0.5	4.9493E-02	4.9492e-02	4.9984e-03	4.9986e-02
0.5	0.5	7.0284E-03	7.0276e-03	7.0388e-03	7.0413e-03
0.9	0.5	9.5762E-04	9.5081e-04	9.5781e-04	9.6304e-04
0.1	0.9	7.0284E-03	7.0205e-03	7.0388e-03	7.0454e-03
0.9	0.9	1.2972E-04	1.3110e-04	1.2972e-04	1.2936e-04

The 3D behavior of numerical values and absolute error is shown in Figures 5 and 6, respectively for $Re = 1$ with $N = 441$. It is observed that numerical values lie between -0.01 to 0.01. The absolute error is found to be of order 10^{-6}, which again implies the applicability of the proposed technique.

Figures 7 and 8 show the behavior of the numerical solution and the absolute error, respectively, for $N = 400$ and $\delta t = 0.001$ with $Re = 10$ and $\alpha = 1$ at $t = 1$. Maximum error is observed

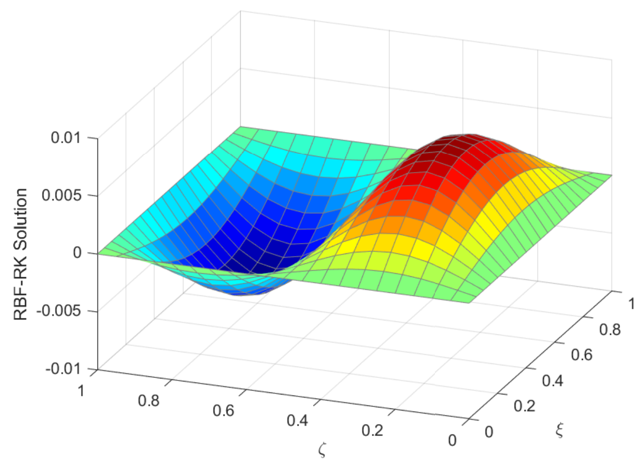

Figure 5: Visualization of numerical solution for Example 1 when $Re = 1$, $\alpha = 1$, $t = 0.1$, $\delta t = 0.001$ and $N = 441$.

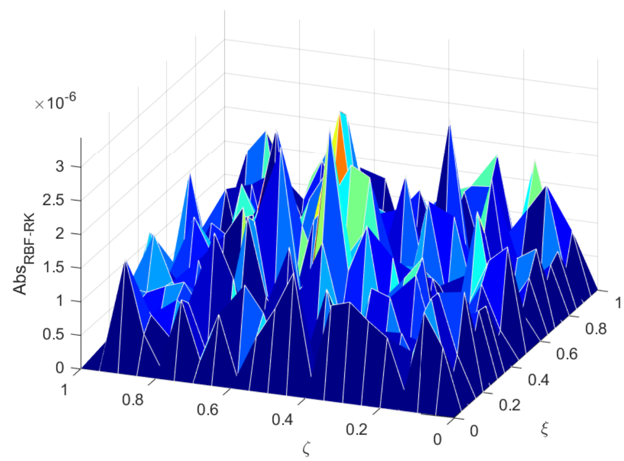

Figure 6: Visualization of absolute error for Example 1 when $Re = 1$, $\alpha = 1$, $t = 0.1$, $\delta t = 0.001$ and $N = 441$.

of order 10^{-5}, which verifies the application of proposed technique. Figures 9–11 imply the active intervention of advection coefficient α in controlling direction of flow. For $\alpha = 0$, the solution profile exhibits multi-directional flow. For $\alpha = 1$, the fluid velocity is directed along single direction, however, for $\alpha = 2$, the fluid flow seems to gradually narrow and concentrate near the origin.

Example 2. Consider the unsteady viscous 2D Burger's equation (19) with initial and boundary data given as follows:

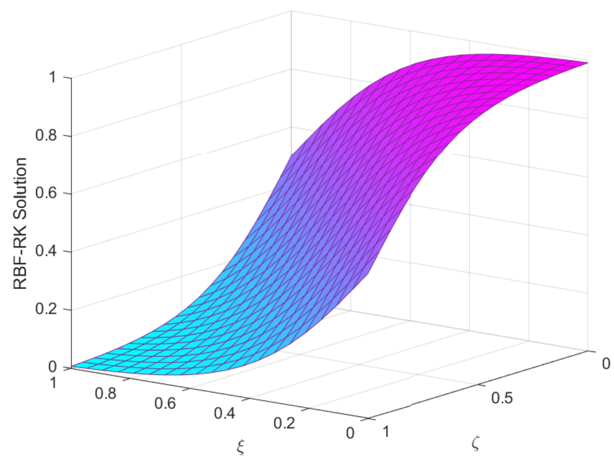

Figure 7: Visualization of numerical solution for Example 1 when $Re = 10$, $\alpha = 1$, $t = 1$, $\delta t = 0.001$ and $N = 400$.

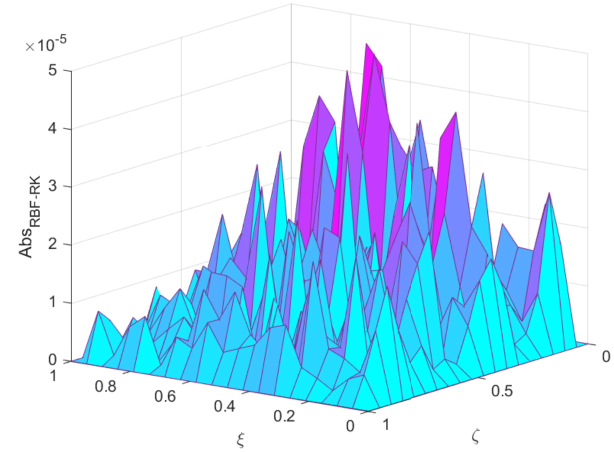

Figure 8: Visualization of absolute error for Example 1 when $Re = 10$, $\alpha = 1$, $t = 1$, $\delta t = 0.001$ and $N = 400$.

$$\vartheta(\xi, \zeta, 0) = \sin(\pi\xi)\sin(2\pi\zeta), \tag{21}$$

where $\Omega = [0, 1] \times [0, 1]$ is the space domain. For the specific case $Re = 1$ and $\alpha = 0$, the analytic solution is mentioned in [32, 38] as follows:

$$\vartheta(\xi, \zeta, t) = \exp(-5t\pi^2)\sin(\pi\xi)\sin(2\pi\zeta). \tag{22}$$

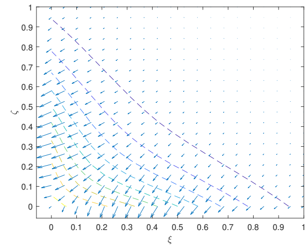

Figure 9: RBF-RK contour profiles for Example 1 when $Re = 1$, $t = 0.5$, $\delta t = 0.001$, $\alpha = 0$ and $N = 400$.

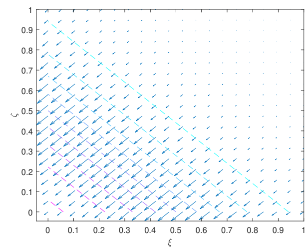

Figure 10: RBF-RK contour profiles for Example 1 when $Re = 1$, $t = 0.5$, $\delta t = 0.001$, $\alpha = 1$ and $N = 400$.

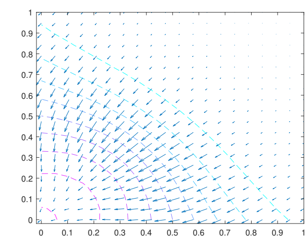

Figure 11: RBF-RK contour profiles for Example 1 when $Re = 1$, $t = 0.5$, $\delta t = 0.001$, $\alpha = 2$ and $N = 400$.

Using initial data given in (21) as initial component in procedure of GB-HPM yields further components of series solution as

$$\begin{aligned}
\vartheta_0(\xi,\zeta,t) =& \sin(\pi\xi)\sin(2\pi\zeta),\\
\vartheta_1(\xi,\zeta,t) =& -(t\sin(\pi\xi)\sin(2\pi\zeta)(5\pi^2 + Re\alpha\pi\cos(\pi\xi)\sin(2\pi\zeta)\\
&+ 2Re\alpha\pi\cos(2\pi\zeta)\sin(\pi\xi)))/Re,\\
\vartheta_2(\xi,\zeta,t) =&(t^2(25\pi^4\sin(\pi\xi)\sin(2\pi\zeta) - Re^2\alpha^2\pi^2\sin(\pi\xi)\sin(2\pi\zeta)^3\\
&- 4Re^2\alpha^2\pi^2\sin(\pi\xi)^3\sin(2\pi\zeta)\\
&- 8Re\alpha\pi^3\cos(\pi\xi)\sin(\pi\xi)(2\cos(2\pi\zeta)^2 - 1)\\
&- 4Re\alpha\pi^3\cos(2\pi\zeta)\sin(2\pi\zeta)(2\cos(\pi x)^2 - 1)
\end{aligned}$$

$$
\begin{aligned}
&+ 14Re\alpha\pi^3 \cos(\pi\xi)\sin(\pi x)\sin(2\pi\zeta)^2 \\
&+ 52Re\alpha\pi^3 \cos(2\pi\zeta)\sin(\pi\xi)^2\sin(2\pi\zeta) \\
&+ 3Re^2\alpha^2\pi^2 \cos(\pi\xi)^2\sin(\pi\xi)\sin(2\pi\zeta)^3 \\
&+ 12Re^2\alpha^2\pi^2 \cos(2\pi\zeta)^2\sin(\pi\xi)^3\sin(2\pi\zeta) \\
&+ 12Re^2\alpha^2\pi^2 \cos(\pi\xi)\cos(2\pi\zeta)\sin(\pi\xi)^2\sin(2\pi\zeta)^2))/(2Re^2), \\
&\vdots
\end{aligned}
$$

Following the same process for $n \geq 2$, the desired number of terms of series solution can be obtained. In the present case, numerical values are computed from the initial five terms of GB-HPM series solution.

For numerical procedures, with the initial condition of a sine waveform, the boundary conditions are set to be periodic as given in (21) and (22). In Table 6, tabulated error norms corresponding to the available exact solution for $\alpha = 0$ and $Re = 1$ are computed by employing different values of N and δt across space-time domain. Accuracy level enhances as step size δt becomes smaller. In Table 7, comparison analysis in terms of absolute error demonstrates the excellence of semi-analytic GB-HPM for very small time $t = 0.001$ and $t = 0.02$. In Table 8, the numerical results are presented for different values of Re and $\alpha = 1$. The agreement between GB-HPM and RBF-RK method signifies the application of proposed techniques on a given 2D Burger's equation.

Table 6: Error norms of RBF-RK solutions of Example 2 for $\alpha = 0$ and $Re = 1$ at various time levels.

			$t = 0.01$		$t = 0.05$		$t = 0.1$	
Method	N	δt	$\|e\|_\infty$	$\|e\|_2$	$\|e\|_\infty$	$\|e\|_2$	$\|e\|_\infty$	$\|e\|_2$
RBF-RK	100	0.001	3.2465e-05	9.9245e-06	1.1422e-05	4.2433e-06	2.6308e-06	8.3001e-07
		0.0001	3.2455e-05	9.9211e-06	1.1415e-05	4.2390e-06	2.6293e-06	8.2940e-07
	441	0.001	1.4088e-06	4.1234e-07	3.1881e-06	8.8184e-07	3.4405e-06	9.4979e-07
		0.0001	1.4088e-06	4.1399e-07	3.1908e-06	8.8215e-07	3.4409e-06	9.4979e-07

However, GB-HPM experiences challenges for $t \geq 0.02$. Therefore, for the aim of small time propagation of physical phenomena such as simulation of earthquake, tsunamis and cosmic dynamics [12, 41, 44], GB-HPM can be an ideal choice. Indeed for further analysis one needs to employ suggested numerical procedures which maintain the standard of accuracy for comparatively large time. In the scenario of lacking an exact solution, mutual comparison of proposed approximate solutions verifies the credibility of the obtained numerical results by the proposed schemes.

Table 7: Numerical results and absolute errors of solutions of Example 2 for $\alpha = 0$ and $Re = 1$.

t	ξ	ζ	GB-HPM	RBF-RK	Abs_{GB-HPM}	Abs_{RBF-RK}
0.001	0.1	0.1	1.7289e-01	1.7290e-01	4.3935e-10	6.8636e-06
	0.5	0.1	5.5948e01	5.5949e-01	1.4218e-09	3.5509e-06
	0.9	0.1	1.7289e-01	1.7289e-01	4.3935e-10	1.0765e-06
	0.3	0.3	7.3237e-01	7.3238e-01	1.8611e-09	6.4155e-06
	0.1	0.9	7.3237e-01	7.3237e-01	1.8611e-09	1.5544e-08
	0.7	0.3	-1.7289e-01	-1.7288e-01	4.3935e-10	6.6740e-06
	0.9	0.9	-1.7289e-09	-1.7289e-01	4.3935e-10	3.3662e-06
0.02	0.1	0.1	6.8911e-02	6.7699e-02	1.2135e-03	2.0509e-06
	0.5	0.1	2.2300e-01	2.1908e-01	3.9271e-03	2.8359e-06
	0.9	0.1	6.8911e-02	6.7699e-02	1.2135e-03	2.1765e-06
	0.3	0.3	2.9191e-01	2.8677e-01	5.1406e-03	2.8133e-06
	0.7	0.3	2.9191e-01	2.8677e-01	5.1406e-03	2.8780e-06
	0.1	0.9	-6.8911e-02	-6.7696e-02	1.2135e-03	1.0952e-06
	0.9	0.9	-6.8911e-02	-6.7696e-02	1.2135e-03	9.0260e-07

Table 8: Numerical results of Example 2 at $\alpha = 1$ and $t = 0.001$ for different Re.

		$Re = 10$		$Re = 100$	
ξ	ζ	GB-HPM	RBF-RK	GB-HPM	RBF-RK
0.1	0.1	1.8014e-01	1.8014e-01	1.8094e-01	1.8095e-01
0.5	0.1	5.8195e-01	5.8196e-01	5.8452e-01	5.8453e-01
0.9	0.1	1.8077e-01	1.8078e-01	1.8158e-01	1.8158e-01
0.3	0.3	7.6548e-01	7.6548e-01	7.6889e-01	7.6889e-01
0.7	0.3	7.6816e-01	7.6816e-01	7.7160e-01	7.7160e-01
0.1	0.9	-1.8077e-01	-1.8078e-01	-1.8158e-01	-1.8158e-01
0.9	0.9	-1.8014e-01	-1.8014e-01	-1.8094e-01	-1.8094e-01

In Figures 12 to 15, RBF-RK solution profiles are shown for $N = 441$ and $\delta t = 0.001$, with the Reynolds number Re varying from 1 to 50. It displays the configuration of sinusoidal waveform. The sinusoidal waveform is generally found in sine curved channels, arteries, alternating current and many more.

7 Conclusion

The present study made an original contribution by conducting a comparative examination of the approximate solutions of two schema classes, namely semi-analytic GB-HPM and numerical collocation methods based on RBFs. Few initial terms of semi-analytic series show adequate convergence to the exact solution and radial basis collocation methods prove their competency along with their complementary meshfree nature. The potential of proposed schemes are compared using absolute, $\|e\|_\infty$ and $\|e\|_2$ error norms for short, moderate and long-time propagation.

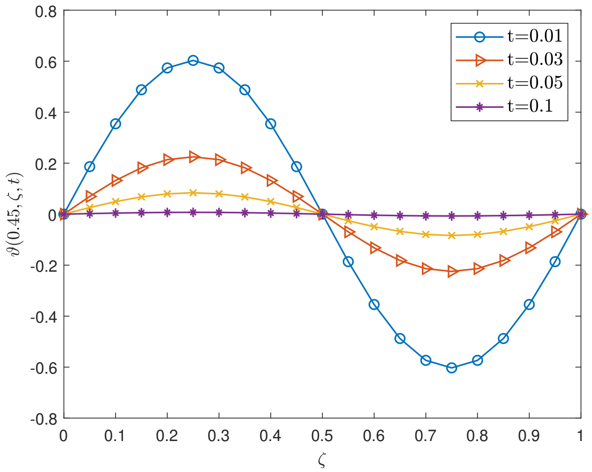

Figure 12: RBF-RK solution profiles of Example 2 when $Re = 1, \alpha = 0$, $\delta t = 0.001$ and $N = 441$.

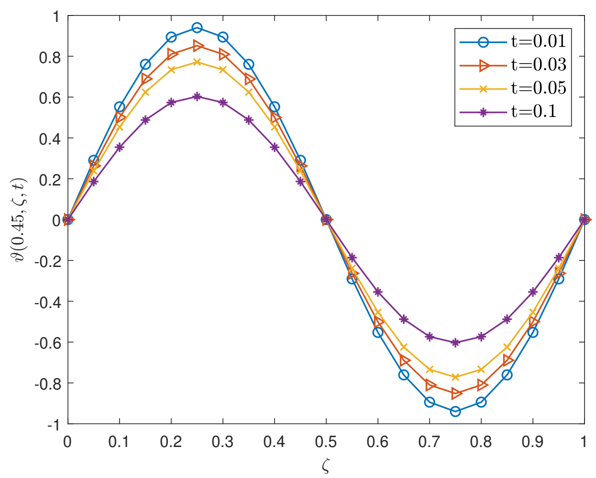

Figure 13: RBF-RK solution profiles of Example 2 when $Re = 10, \alpha = 0$, $\delta t = 0.001$ and $N = 441$.

The GB-HPM exhibits promising accuracy for short and moderate-time propagation but fails to maintain its standard for long-time computations. However at cost of some more computational efforts suggested numerical scheme has performed pretty well at all time levels.

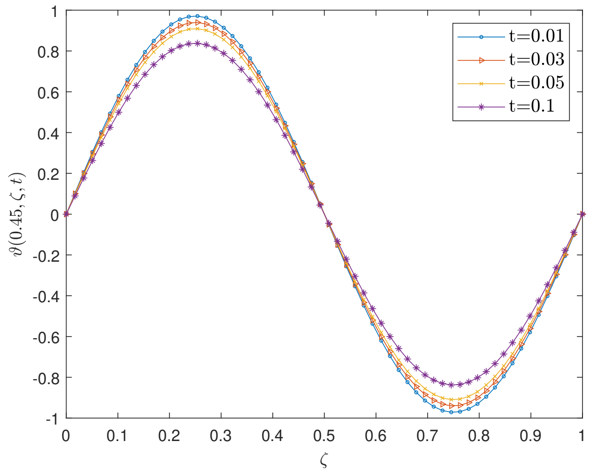

Figure 14: RBF-RK solution profiles of Example 2 when $Re = 30, \alpha = 0$, $\delta t = 0.001$ and $N = 441$.

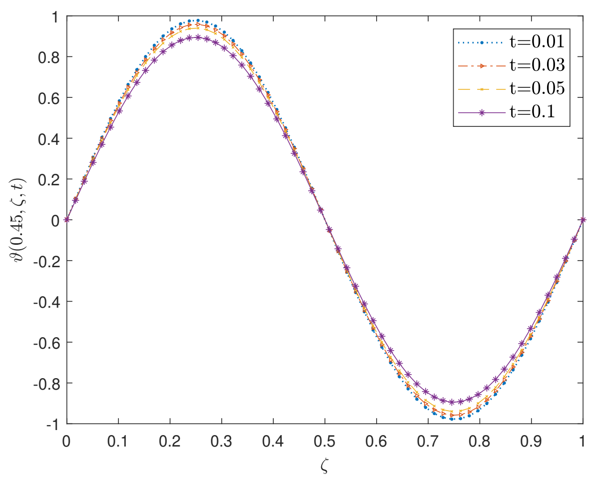

Figure 15: RBF-RK solution profiles of Example 2 when $Re = 50, \alpha = 0$, $\delta t = 0.001$ and $N = 441$.

Funding

Dr. Shelly Arora is thankful to DST-ANRF for providing grant via SPG/2022/001269 and Ms. Amandeep Kaur is thankful to CSIR for providing Junior Research Fellowship F. No. 09/0140(17151)/2023-EMR-I.

Conflicts of Interest

All authors jointly worked on the results and they read and approved the final manuscript and also declare that they have no competing interests.

References

[1] Arora, G., and Joshi, V. *A computational approach using modified trigonometric cubic B-spline for numerical solution of Burger's equation in one and two dimensions*, Alex. Eng. J. 57(2) (2018), 1087–1098.

[2] Arora, S., Dhaliwal, S.S. Ma, W.X., and Pasrija, A. *Analysis of fractional order Schrodinger equation with singular and nonsingular kernel derivatives via novel hybrid scheme*, J. Appl. Anal. Comput. 15(2) (2025), 1039–1067.

[3] Arora, S., and Pasrija, A. *A novel integral transform operator and its applications,* Iran. J. Numer. Anal. Optim. 13(3) (2023), 553–575.

[4] Babu, A., Han, B., and Asharaf, N., *Numerical solution of the viscous Burger's equation using localized differential quadrature method*, Partial Differ. Equ. Appl. Math. 4 (2021), 100044.

[5] Bahadır, A.R. *A fully implicit finite-difference scheme for two-dimensional Burger's equations*, Appl. Math. Comput. 137(1) (2003), 131–137.

[6] Bateman, H. *Some recent researches on the motion of fluids*, Mon. Weather Rev. 43(4) (1915), 163–170.

[7] Biazar, J., and Hosami, M. *An interval for the shape parameter in radial basis function approximation*, Appl. Math. Comput. 315 (2017), 131–149.

[8] Bilige, S., and Chaolu, T. *An extended simplest equation method and its application to several forms of the fifth-order KdV equation*, Appl. Math. Comput. 216(11) (2010), 3146–3153.

[9] Bonkile, M.P., Awasthi, A., Lakshmi, C., Mukundan, V., and Aswin, V.S. *A systematic literature review of Burger's equation with recent advances*, Pramana, 90 (2018), 1-21.

[10] Breuer, H.P., and Petruccione, F. *Burger's model of turbulence as a stochastic process*, J. Phys. A. 25(11) (1992), L661.

[11] Burger, M., Göttlich, S. and Jung,T. *Derivation of second order traffic flow models with time delays*, Netw. Heterog. Media. 14(2) (2019), 265–288.

[12] Carcione, J.M., Poletto, F., Farina, B., and Craglietto, A. *Simulation of seismic waves at the Earth's crust (brittle–ductile transition) based on the Burger's model*, Solid Earth, 5(2) (2014), 1001–1010.

[13] Carlson, R.E., and Foley, T.A. *The parameter R2 in multiquadric interpolation*, Comput. Math. Appl. 21(9) (1991), 29–42.

[14] Fasshauer, G.E. *Newton iteration with multiquadrics for the solution of nonlinear PDEs*, Comput. Math. Appl. 43(3-5) (2002), 423–438.

[15] Fasshauer, G.E., and Zhang, J.G. *On choosing "optimal" shape parameters for RBF approximation*, Numer. Algorithms, 45 (2007), 345–368.

[16] Franke, R., *Scattered data interpolation: tests of some methods*, Math. Comput. 38:157 (1982), 181–200.

[17] Gardner, C.S., Greene, J.M., Kruskal, M.D., and Miura, R.M. *Method for solving the Korteweg-deVries equation*, Phys. Rev. Lett. 19(19) (1967), 1095.

[18] Hardy, R.L. *Theory and applications of the multiquadric-biharmonic method 20 years of discovery 1968–1988*, Comput. Math. Appl. 19(8-9) (1990), 163–208.

[19] Hirota, R., and Satsuma, J. *Nonlinear evolution equations generated from the Bäcklund transformation for the Boussinesq equation*, Prog. Theor. Phys. 57(3) (1977), 797–807.

[20] Jafari, H., Tajadodi, H., and Baleanu, D. *Application of a homogeneous balance method to exact solutions of nonlinear fractional evolution equations*, J. Comput. Nonlinear Dyn. 9(2) (2014), 021019.

[21] Jain, P.C., and Holla, D.N. *Numerical solutions of coupled Burger's equation*, Int. J. Non-Linear Mech. 13(4) (1978), 213–222.

[22] Jawad, A.J.A.M. *The sine-cosine function method for the exact solutions of nonlinear partial differential equations*, Sys. 2(3) (2012) 1.

[23] Kadkhoda, N., and Jafari, H., *Kudryashov method for exact solutions of isothermal magnetostatic atmospheres*, Iran. J. Numer. Anal. Optim. 6(1) (2016), 43–53.

[24] Kansa, E.J., *Multiquadrics—A scattered data approximation scheme with applications to computational fluid-dynamics—I surface approximations and partial derivative estimates*, Comput. Math. Appl. 19(8-9) (1990), 127–145.

[25] Kansa, E.J., and Holoborodko, P. *On the ill-conditioned nature of C^∞ RBF strong collocation*, Eng. Anal. Bound. Elem. 78 (2017), 26–30.

[26] Kumar, N., Verma, A.K., and Agarwal, R.P. *Two-Dimensional Uniform and Non-Uniform Haar Wavelet Collocation Approach for a Class of Nonlinear PDEs*, Comput. 11(10) (2023), 189.

[27] Li, M., Nikan, O., Qiu, W., and Xu, D. *An efficient localized meshless collocation method for the two-dimensional Burger's-type equation arising in fluid turbulent flows*, Eng. Anal. Bound. Elem. 144 (2022), 44–54.

[28] Liu, Z., and Yang, C. *The application of bifurcation method to a higher-order KdV equation*, J. Math. Anal. Appl. 275(1) (2002), 1–12.

[29] Lombard, B., and Matignon, D. *Diffusive approximation of a time-fractional Burger's equation in nonlinear acoustics*, SIAM J. Appl. Math. 76(5) (2016), 1765–1791.

[30] Ma, W.X., Huang, T., and Zhang, Y. *A multiple exp-function method for nonlinear differential equations and its application*, Phys. Scr. 82(6) (2010), 065003.

[31] Mittal, R.C., and Jiwari, R. *A differential quadrature method for numerical solutions of Burger's-type equations*, Int. J. Numer. Methods Heat Fluid Flow. 22(7) (2012), 880–895.

[32] Mittal, R.C., and Tripathi, A. *Numerical solutions of two-dimensional Burger's equations using modified Bi-cubic B-spline finite elements*, Eng. Comput. 32(5) (2015), 1275–1306.

[33] Mohamed, N.A. *Solving one-and two-dimensional unsteady Burger's equation using fully implicit finite difference schemes*, Arab J. Basic Appl. Sci. 26(1) (2019), 254–268.

[34] Mohanty, S.K., Kumar, S., Dev, A.N., Deka, M.K., Churikov, D.V., and Kravchenko, O.V. *An efficient technique of G'/ G–expansion method for modified KdV and Burger's equations with variable coefficients*, Result. Phys. 37 (2022), 105504.

[35] Mojtabi, A., and Deville, M.O. *One-dimensional linear advection–diffusion equation: Analytical and finite element solutions*, Comput. Fluids. 107 (2015), 189–195.

[36] Nofal, T.A. *Simple equation method for nonlinear partial differential equations and its applications*, Int. J. Egypt. Math. Soc. 24(2) (2016), 204–209.

[37] Ozer, S. and Kutluay, S. *An efficient and reliable numerical study for the 2D nonlinear coupled Burgers equation simulating many physical phenomena.*Int. J. Mod. Phys. C. 37(1) (2026), 2550051.

[38] Radwan, S.F. *Comparison of higher-order accurate schemes for solving the two-dimensional unsteady Burger's equation*, J. Comput. Appl. Math. 174(2) (2005), 383–397.

[39] Rippa, S., *An algorithm for selecting a good value for the parameter c in radial basis function interpolation*, Adv. Comput. Math., 11 (1999), 193–210.

[40] Sarra, S.A., and Kansa, E.J. *Multiquadric radial basis function approximation methods for the numerical solution of partial differential equations*, Adv. Comput. Mech. 2(2) (2009), 220.

[41] Satake, K. *Tsunamis*, In International geophysics, vol. 81, pp. 437-451. Academic press, 2002.

[42] Wacławczyk, M., and Oberlack, M. *Application of the extended Lie group analysis to the Hopf functional formulation of the Burger's equation*, J. Math. Phys. 54(7) (2013).

[43] Wazwaz, A.M. *Multiple-soliton solutions for the KP equation by Hirota's bilinear method and by the tanh-coth method*, Appl. Math. Comput. 190(1) (2007), 633–640.

[44] Webb, G.M. and McKenzie, J.F. *Burger's equation and cosmic ray shocks*, J. Plasma Phys. 31(3) (1984), 337–368.

[45] Xu, S., He, J., and Wang, L. *The Darboux transformation of the derivative nonlinear Schrödinger equation*, J. Phys. A: Math. Theor. 44(3)0 (2011), 305203.